

# Heat radiation from long cylindrical objects

Vladyslav A. Golyk, Matthias Krüger, and Mehran Kardar

*Massachusetts Institute of Technology, Department of Physics, Cambridge, Massachusetts 02139, USA*

The heat radiated by objects small or comparable to the thermal wavelength can be very different from the classical blackbody radiation as described by the laws of Planck and Stefan-Boltzmann. We use methods based on scattering of electromagnetic waves to explore the dependence on size, shape, as well as material properties. In particular, we explore the radiation from a long cylinder at uniform temperature, discussing in detail the degree of polarization of the emitted radiation. If the radius of the cylinder is much smaller than the thermal wavelength, the radiation is polarized parallel to the cylindrical axis and becomes perpendicular when the radius is comparable to the thermal wavelength. For a cylinder of uniaxial material (a simple model for carbon nanotubes), we find that the influence of uniaxiality on the polarization is most pronounced if the radius is larger than a few microns, and quite small for submicron sizes typical for nanotubes.

PACS numbers: 12.20.-m, 44.40.+a, 05.70.Ln

## I. INTRODUCTION

Thermal radiation lies at the heart of modern statistical physics and goes back to the beginnings of quantum mechanics more than a century ago [1]. Planck's law describes the intensity  $\mathcal{I}$  (per unit surface area and solid angle) of radiation of a black body at temperature  $T$

$$\mathcal{I} = \frac{\hbar\omega^3}{2\pi^2c^2} \frac{1}{e^{\frac{\hbar\omega}{k_B T}} - 1}. \quad (1)$$

Here,  $\omega$  is the angular frequency of radiation and  $\hbar$  and  $c$  are reduced Planck's constant and the speed of light, respectively. Integration over angles and frequencies yields the well known Stefan-Boltzmann law[2] for the total power  $H$  radiated per unit area  $A$ ,

$$H/A = \sigma T^4, \quad (2)$$

with  $\sigma = \pi^2 k_B^4 / (60\hbar^3 c^2)$ .

Only recently, various phenomena, leading to modifications of these laws have been explored. For example, the effect of spatial coherence of emitted heat radiation was studied by many authors [3–6] as this effect can be used in many technological applications [7–10], such as thermophotovoltaic and high-efficiency light sources.

For real materials, Eq. (1) can be adjusted by introducing the (angle dependent) emissivity of the material, which is unity for a black body. Considering objects with sizes smaller or comparable to the thermal wavelength  $\lambda_T = \hbar c / k_B T$  (approximately  $7.6 \mu\text{m}$  at room temperature), the radiated energy differs from the above equations because of interference effects of the object with the emitted radiation. In other words, the emissivity then depends on the size and shape of the object. Additionally, if the object is smaller than the penetration (skin) depth, the emitted power is proportional to the object's volume, rather than surface area. The heat radiation of small spherical objects including these effects have been studied since the 1970s[11, 12]. Also, effects of excitations[13] and electric currents[14] on the radiation have been studied. Furthermore, recent studies on

superscattering properties of subwavelength nanostructures (e.g. nanorods)[15] make such systems potential candidates for efficient heat transfer sources.

Experimentally, the radiation of thin cylindrical objects with thickness in the range of the thermal wavelength is very well accessible, and has e.g. been studied using metal wires with interesting findings: 50 years ago, it was discovered that the radiation of a hot thin metal wire is significantly polarized [16]. Polarizations of 28% [16] and 50% [17] in the direction perpendicular to the wire were measured for thin incandescent tungsten and silver wires respectively. In both studies the thickness of the wires was larger or comparable to the thermal wavelengths. These findings triggered a number of studies on the properties of thermal radiation of sources of various designs, including platinum microwires [18, 19], semiconductor layers in external magnetic fields [20], bundles of carbon nanotubes [21, 22] and SiC lamellar gratings [23].

For wires with thickness smaller or comparable to the thermal wavelength, the radiation was found (e.g. for platinum) to be polarized in the direction parallel to the wire becoming fully polarized as the width approaches zero [18, 19]. Polarization effects have also been observed for radiation of bundles of carbon nanotubes [21] and are considered a simple way of finding the degree of alignment inside the bundle. For carbon nanotubes, an explanation for this polarization, taking into account the electronic structure of the tubes, has been discussed in Ref. [22].

Recent work on the heat radiation of thin metal wires [24] provides experimental as well as theoretical results, albeit restricted to emission perpendicular to the cylindrical axis. Also, a series of works [25–27] discuss radiation emitted by individual incandescent carbon nanotubes. In Ref. [26], the polarization of the radiation is studied both experimentally and theoretically using a model based on Mie theory.

In this paper, we provide the general formalism to compute the heat radiation of arbitrary objects in terms of their classical scattering properties, which is part of the general framework [28] for non-equilibrium electro-

magnetic fluctuations involving multiple objects and arrays [29–35]. Thereby we give a more extensive derivation of the corresponding results presented in Ref.[28], which is also more general in terms of material properties: We include the possibility of dielectric or magnetic losses, locality or non-locality. Additionally, we provide a new, simpler, formalism to derive the heat radiation (see Eq. (19) below). To this end, we start from quantum thermal fluctuations inside the object following the theory of fluctuational electrodynamics introduced over 60 years ago by Rytov [36]. Then, we derive the heat radiation of the experimentally important case of a cylindrical object, discussing polarization effects for different conducting and insulating materials, as well as asymptotic limits. This detailed discussion hence provides much deeper understanding of material and size effects compared to the brief introduction of dielectric cylinders in Ref. [28]. We derive the so far unknown heat radiation of a cylinder made of uniaxial material, where the symmetry axis of the material and the cylinder coincide. We apply this formula to introduce a simple model for the heat radiation of multi-walled carbon nanotubes (MWCNT).

The paper is composed as follows: In section II, we give the general formalism for heat radiation of arbitrary objects and apply it to the cases of a cylindrical object. Additionally, we find the radiation of an anisotropic plate, generalizing the known results [36] for the isotropic case. Sec. III finally gives the specific form of the scattering operator for a cylinder made of uniaxial material, needed to evaluate the formula of Sec. II B. In Sec. IV, we discuss the total radiated energy by cylinders made of different materials, such as dielectrics, metals, and MWCNT, putting special focus on the degree of polarization of the radiation. Finally, in Sec. V, we discuss the spectral density of the energy emitted by these materials, a quantity which might be most accessible in experiments. We close with a summary and discussion of our findings in Sec. VI.

## II. HEAT RADIATION IN TERMS OF SCATTERING OPERATOR

### A. General formalism for arbitrary objects

Consider an object with homogeneous temperature  $T_{obj}$  placed in vacuum, enclosed by an environment (e.g. a cavity much larger than all other scales in the system) at temperature  $T_{env}$ . In global equilibrium, i.e. with  $T_{obj} = T_{env} = T$ , the autocorrelation function  $C$  of the electric field is related to the imaginary part of the dyadic Green's function  $G_{ij}$  of the object by the fluctuation-dissipation theorem (FDT) [36, 37],

$$\begin{aligned} C_{ij}^{eq}(T) &\equiv \langle E_i(\omega; \mathbf{r}) E_j^*(\omega; \mathbf{r}') \rangle^{eq} \equiv \langle \mathbf{E}(\omega; \mathbf{r}) \otimes \mathbf{E}^*(\omega; \mathbf{r}') \rangle_{ij}^{eq} \\ &= [a_T(\omega) + a_0(\omega)] \frac{c^2}{\omega^2} \text{Im} G_{ij}(\omega; \mathbf{r}, \mathbf{r}'), \end{aligned} \quad (3)$$

where  $\otimes$  denotes a dyadic product.  $a_T(\omega) \equiv \frac{\omega^4 \hbar (4\pi)^2}{c^4} (\exp[\hbar\omega/k_B T] - 1)^{-1}$  describes the thermal contribution to quantum fluctuations, compare Eq. (1). The zero point fluctuations, which contribute  $a_0(\omega) \equiv \frac{\omega^4 \hbar (4\pi)^2}{2c^4}$ , are independent of the object's temperature and do not contribute to heat radiation. Hereafter we use the operator notation  $\mathbb{G} \equiv G_{ij}(\omega; \mathbf{r}, \mathbf{r}')$ , where operator multiplication implies an integration over space as well as a  $3 \times 3$  spatial matrix multiplication, e.g. for the operators  $\mathbb{A}$  and  $\mathbb{B}$  (using Einstein summation convention),

$$(\mathbb{A}\mathbb{B})_{ik}(\mathbf{r}, \mathbf{r}') = \int d^3 r'' A_{ij}(\mathbf{r}, \mathbf{r}'') B_{jk}(\mathbf{r}'', \mathbf{r}'). \quad (4)$$

The Green's function is the solution of [38, 39]

$$\left[ \mathbb{H}_0 + \mathbb{V} - \frac{\omega^2}{c^2} \mathbb{I} \right] \mathbb{G} = \mathbb{I}, \quad (5)$$

which follows because the electric field obeys the Helmholtz equation, Eq. (9) below. Here,  $\mathbb{H}_0 = \nabla \times \nabla \times$  describes free space, and  $\mathbb{V} = \frac{\omega^2}{c^2} (\mathbb{I} - \epsilon + \nabla \times \left( \frac{1}{\mu} - \mathbb{I} \right) \nabla \times)$  is the potential introduced by the object.  $\epsilon$  and  $\mu$  are the complex (possibly nonlocal) dielectric permittivity and magnetic permeability tensors of the object. For isotropic and local materials, they reduce to scalars (e.g.  $\epsilon = \epsilon \mathbb{I}$ ).  $\mathbb{G}_0$  is the Green's function of free space. Using the identities  $\text{Im} \mathbb{G} = -\mathbb{G} \text{Im} \mathbb{G}^{-1} \mathbb{G}^*$  and  $\text{Im} \mathbb{V} = \text{Im}(\mathbb{G}^{-1} - \mathbb{G}_0^{-1})$  [37], which can be found from Eq. (5), we obtain

$$C^{eq}(T) = C_0 + C(T) - a_T(\omega) \frac{c^2}{\omega^2} \mathbb{G} \text{Im} \mathbb{G}_0^{-1} \mathbb{G}^*, \quad (6)$$

$$\begin{aligned} C(T_{obj}) &= -a_{T_{obj}}(\omega) \frac{c^2}{\omega^2} \mathbb{G} \text{Im} \mathbb{V} \mathbb{G}^* \\ &= -a_{T_{obj}}(\omega) \frac{c^2}{\omega^2} \int_{obj} d^3 r' d^3 r'' G_{ij}(\mathbf{r}, \mathbf{r}') \\ &\quad \times \text{Im} V_{jk}(\mathbf{r}', \mathbf{r}'') G_{kl}^*(\mathbf{r}'', \mathbf{r}'''), \end{aligned} \quad (7)$$

where  $C_0 = a_0(\omega) \frac{c^2}{\omega^2} \text{Im} \mathbb{G}$  is the zero point term. Equation (6) shows two different finite temperature contributions to the electric field in equilibrium.  $C(T)$  contains an explicit integral over the sources within the object, as  $\text{Im} \mathbb{V}$  is only nonzero inside the object, and we identify it with the desired heat radiation from the object. The expression in Eq. (7) can be shown to be identical to expressions in the literature for both complex electric and magnetic permeabilities [36, 37], where, in general, one has two terms, including  $\text{Im} \epsilon$  and  $\text{Im} \mu$ , respectively. The introduction of the potential  $\mathbb{V}$  appears useful here, as it allows for a compact notation including both terms. The third term in Eq. (6),

$$C^{env}(T_{env}) = -a_{T_{env}}(\omega) \frac{c^2}{\omega^2} \mathbb{G} \text{Im} \mathbb{G}_0^{-1} \mathbb{G}^*, \quad (8)$$

is the contribution sourced by the environment. As a specific model for environment, consider the objects enclosed in a very large black cavity maintained at temperature  $T_{env}$ . This latter identification can be corroborated on a different route by introducing a cold object

into the thermal background field  $\mathbf{E}_0$  sourced by the environment, with field correlator given by  $\langle \mathbf{E}_0 \otimes \mathbf{E}_0^* \rangle = a_{T_{env}}(\omega) \frac{c^2}{\omega^2} \text{Im} \mathbb{G}_0$ . At this point, it is useful to introduce the  $\mathbb{T}$  operator or scattering amplitude  $\mathbb{T}$  [38, 40] of the object. It relates the homogeneous solution (also sometimes called the exciting field [40])  $\mathbf{E}_h$  (for  $\mathbb{V} = 0$ ) of the Helmholtz equation

$$\left[ \mathbb{H}_0 + \mathbb{V} - \frac{\omega^2}{c^2} \mathbb{I} \right] \mathbf{E} = 0, \quad (9)$$

to its (inhomogeneous) solution  $\mathbf{E}_{ih}$  with the object present. This solution can be stated in terms of the Lippmann-Schwinger equation

$$\mathbf{E}_{ih} = (1 - \mathbb{G}_0 \mathbb{T}) \mathbf{E}_h. \quad (10)$$

With this equation, the above introduction of the cold object into the free environment field is readily done and  $C^{env}$  is then the correlator of the field  $\mathbf{E}_s$ , the inhomogeneous solution with the object present,

$$\begin{aligned} C^{env}(T_{env}) &= \langle \mathbf{E}_s \otimes \mathbf{E}_s^* \rangle = (1 - \mathbb{G}_0 \mathbb{T}) \langle \mathbf{E}_0 \otimes \mathbf{E}_0^* \rangle \\ &\times (-\mathbb{T}^* \mathbb{G}_0^* + 1) = -a_{T_{env}}(\omega) \frac{c^2}{\omega^2} \mathbb{G} \text{Im} \mathbb{G}_0^{-1} \mathbb{G}^*, \end{aligned} \quad (11)$$

in agreement with Eq. (8). Here we used the identity [38]

$$\mathbb{G} = \mathbb{G}_0 - \mathbb{G}_0 \mathbb{T} \mathbb{G}_0. \quad (12)$$

Equation (11) highlights the physical interpretation of  $C^{env}$ : It is the radiation sourced by the environment and scattered by the object.

Having found the contributions of the different sources (environment and object), one can now vary the temperature of these independently in order to arrive at the field outside the object when its temperature is different from that of the environment. If  $T_{env} = 0$  this field corresponds to the heat radiation of the object. To this end, we notice that it is not necessary to derive all the terms in Eq. (6) as explained in the following: The explicit expression for  $C(T_{obj})$  in Eq. (7) contains the Green's function with one argument inside and one argument outside the object. While this function can be in principle derived, we find it more convenient to express  $C(T_{obj})$  in terms of the Green's function with both arguments outside the object, as it is directly linked to the scattering operator by Eq. (12). Therefore, it is interesting to note that  $C^{env}$  has all the sources outside the object and hence can be found in terms of this Green's function. While this is already obvious in Eq. (11) we additionally present a more rigorous way to derive  $C^{env}$ . The environment sources, described by  $\varepsilon_{env}$ , can be thought of as being everywhere in the infinite space complementary to the object, infinitesimal in strength (environment ‘‘dust’’ [37]), i.e.  $\varepsilon_{env} \rightarrow 1$ .  $C^{env}$  in Eq. (8) can hence be written

$$\begin{aligned} C^{env}(T_{env}) &= a_{T_{env}}(\omega) \\ \lim_{\varepsilon_{env} \rightarrow 1} \int_{\text{outside}} d^3 r' \tilde{G}_{ik}(\mathbf{r}, \mathbf{r}') \text{Im} \varepsilon_{env} \tilde{G}_{jk}^*(\mathbf{r}'', \mathbf{r}'), \end{aligned} \quad (13)$$

which is identical to Eq. (4) in Ref. [28]. Here, we introduced a Green's function  $\mathbb{G}$  with  $\mathbb{V}$  inside the object and  $\varepsilon_{env}$  outside. This is a simple modification of  $\mathbb{G}$  as a finite  $\varepsilon_{env} - 1$  only changes the external speed of light so that  $c$  in  $\mathbb{G}$  is replaced by  $c/\sqrt{\varepsilon_{env}}$ .

Finally the heat radiation of the object at temperature  $T_{obj}$  can now be found by solving Eq. (6) for  $C(T_{obj})$ ,

$$C(T_{obj}) = a_{T_{obj}}(\omega) \frac{c^2}{\omega^2} \text{Im} \mathbb{G} - C^{env}(T_{obj}), \quad (14)$$

where  $\mathbb{G}$  is found using Eq. (12). Note that  $C^{env}(T)$  can be derived from either Eq. (13) or directly from Eq. (11). For the case of the cylinder, we present below the former derivation in detail, and briefly sketch the latter starting from Eq. (11).

We emphasize again that the field emitted by the object in Eq. (14) is fully expressed in terms of the Green's function with both arguments outside the object. In case one is only interested in the total heat emitted, the first term, i.e., the equilibrium field need not be derived, as it contains no Poynting vector. If, on the other hand, the radiation of the object is scattered at other objects, e.g. in order to compute heat transfer or nonequilibrium Casimir interactions, the full expression (14) has to be kept.

## B. Heat radiation of a cylindrical object

In order to compute the heat radiation of a cylindrical object (denoted by subscripts  $c$ ), we apply Eq. (14), evaluating the environment contribution by use of Eq. (13). Afterwards in this subsection, we briefly sketch the derivation via Eq. (11). In the cylindrical geometry (with parallel, radial and angular coordinates  $z$ ,  $r$  and  $\phi$ , respectively), the free Green's function  $\mathbb{G}_0$  is expanded in cylindrical vector waves,  $\mathbf{RM}_{n,k_z}$  and  $\mathbf{RN}_{n,k_z}$  corresponding to  $M$ -polarized and  $N$ -polarized regular waves [40], see App. A. These are indexed by the multipole order  $n$  and  $k_z$ , the component of the wavenumber  $k = \omega/c$  along the cylindrical axis. For outgoing waves we use  $\mathbf{M}_{n,k_z}$  and  $\mathbf{N}_{n,k_z}$  accordingly. In this basis, the  $\mathbb{T}$  operator of a cylindrical object is diagonal in  $n$  and  $k_z$ , but couples different polarizations. Its entry  $T_{n,k_z}^{P'P}$  relates the amplitude of a scattered wave of polarization  $P'$  in response to an incoming wave of unit amplitude and polarization  $P$ , with  $P, P' \in \{M, N\}$ . More precisely, the application of the  $\mathbb{T}$  operator in Eq. (10) on regular cylindrical functions reads,

$$-\mathbb{G}_0 \mathbb{T}_c \mathbf{R} \mathbf{P}_{n,k_z} = \sum_{P'} T_{n,k_z}^{P'P} \mathbf{P}'_{n,k_z}. \quad (15)$$

With these definitions and Eq. (A.2), the Green's function of the cylinder is easily found, by use of Eq. (12),

as

$$\mathbb{G}_c = \mathbb{G}_0 - \mathbb{G}_0 \mathbb{T}_c \mathbb{G}_0 = \mathbb{G}_0 + \sum_{P, P'} \sum_{n=-\infty}^{\infty} (-1)^n \int_{-\infty}^{\infty} \frac{ik_z}{8\pi} \mathbf{P}_{n, k_z}(\mathbf{r}) \otimes \mathbf{P}'_{-n, -k_z}(\mathbf{r}') T_{n, k_z}^{PP'}.$$
 (16)

When performing the integration in Eq. (13), we note that  $\mathbb{G}_0(\mathbf{r}, \mathbf{r}')$  in Eq. (A.2) is separated into two pieces, corresponding to  $r < r'$  and  $r' < r$ . The contribution of a finite region vanishes asymptotically in the limit of  $\varepsilon_{env} \rightarrow 1$  and can thus be neglected without changing the result. We can hence restrict the integration range to  $r' \geq r, r''$ , where we have to use exclusively one of the pieces. In general, one can restrict the integration in Eq. (13) to  $\xi(\mathbf{r}') \geq \xi(\mathbf{r}), \xi(\mathbf{r}'')$ , where  $\xi$  is the component which distinguishes the two expansions of  $\mathbb{G}_0$ .

Due to the orthogonality of two basis sets of the wave functions, the integrations over polar angle  $\phi'$  and cylin-

drical axis  $z'$  yield  $2\pi\delta_{n, n'}$  and  $2\pi\delta(k_z - k'_z)$ , respectively, and we are left with only one term for each polarization in Eq. (13),

$$\lim_{\varepsilon_{env} \rightarrow 1} \int r' dr' \left| \tilde{\mathbf{P}}_{-n, -k_z}(\mathbf{r}') \right|^2 = \frac{2c^2}{\pi\omega^2} \frac{1}{\text{Im}\varepsilon_{env}} + \dots,$$
 (17)

where  $\tilde{\mathbf{P}}_{n, k_z}$  has analogous form to  $\mathbf{P}_{n, k_z}$  with the wavenumber  $\sqrt{\varepsilon_{env}}\omega/c$  instead of  $\omega/c$ . Also, “...” represent higher order terms in  $\varepsilon_{env} - 1$ . This equation holds for  $k_z^2 < \omega^2/c^2$ , for  $k_z^2 > \omega^2/c^2$  all terms are of order  $\varepsilon_{env}^0$  and do not contribute in Eq. (13), a manifestation of the fact that the environment radiation does not contain evanescent waves.

The radiation from the environment after scattering at the cylinder then reads

$$C_c^{env}(T_{env})(\mathbf{r}, \mathbf{r}'') = a_{T_{env}}(\omega) \sum_{P, P'} \sum_{n=-\infty}^{\infty} \int_{-\omega/c}^{\omega/c} \frac{dk_z}{8\pi} \frac{c^2}{\omega^2} \left\{ \mathbf{R}\mathbf{P}_{n, k_z}(\mathbf{r}) \otimes \mathbf{R}\mathbf{P}'_{n, k_z}(\mathbf{r}'') \delta_{P, P'} + \mathbf{R}\mathbf{P}_{n, k_z}(\mathbf{r}) \otimes \mathbf{P}'_{n, k_z}(\mathbf{r}'') T_{n, k_z}^{P'P^*} \right. \\ \left. + \mathbf{P}_{n, k_z}(\mathbf{r}) \otimes \mathbf{R}\mathbf{P}'_{n, k_z}(\mathbf{r}'') T_{n, k_z}^{PP'} + \mathbf{P}_{n, k_z}(\mathbf{r}) \otimes \mathbf{P}'_{n, k_z}(\mathbf{r}'') \sum_{P''} T_{n, k_z}^{PP''} T_{n, k_z}^{P''P^*} \right\},$$
 (18)

where  $\bar{P}$  stands for the polarization opposite to  $P$ . Physically, Eq. (18) describes the thermal field for the case of an environment at temperature  $T_{env}$  and a cold cylinder ( $T_c = 0$ ). It can also be derived via Eq. (11), by noting that the radiation of the environment without cylinder present can be given in closed form,

$$\langle \mathbf{E}_0 \otimes \mathbf{E}_0^* \rangle = a_{T_{env}}(\omega) \frac{c^2}{\omega^2} \text{Im} \mathbb{G}_0 = a_{T_{env}}(\omega) \sum_P \sum_{n=-\infty}^{\infty} \int_{-\omega/c}^{\omega/c} \frac{dk_z}{8\pi} \frac{c^2}{\omega^2} [\mathbf{R}\mathbf{P}_{n, k_z} \otimes \mathbf{R}\mathbf{P}_{n, k_z}^*].$$
 (19)

Application of  $(1 - \mathbb{G}_0 \mathbb{T}_c)$  from both sides (compare Eq. (11)), using Eq. (15) immediately leads to Eq. (18). This simple route towards the environment radiation (and hence the radiation of the object) has not been presented before.

Since we are only interested in the energy emitted by the cylinder, we do not explicitly derive the equilibrium field in Eq. (14) as it contains no Poynting vector. Equation (14) thus states Kirchhoff's law, that the energy absorbed by the cylinder in the case  $T_{env} = T, T_c = 0$  is the same as the energy radiated by it for  $T_{env} = 0, T_c = T$ . This is a special case of detailed balance in equilibrium,

which generally states that the absorption coefficient of an object equals its emission coefficient. The formalism described here hence also provides a convenient route to find the absorption coefficient of arbitrary objects. Technically, due to these considerations, the Poynting vector

$$\langle \mathbf{S}(\mathbf{r}) \rangle = \frac{c}{4\pi} \int \frac{d\omega}{(2\pi)^2} \text{Re} [\langle \mathbf{E}(\omega, \mathbf{r}) \times \mathbf{H}^*(\omega, \mathbf{r}) \rangle],$$
 (20)

of the field in Eq. (18) gives complete information about the net energy flux for any temperature combinations. It can be derived via  $\mathbf{B}(\omega, \mathbf{r}) = \frac{-ic}{\omega} \nabla \times \mathbf{E}(\omega, \mathbf{r})$  as well as relation (A.3). The power  $|H_c|$  radiated per length  $L$  of the infinite cylinder in the general case of finite  $T_{env}$  and  $T_c$  is finally given by [28],

$$\frac{|H_c|}{L} = -\frac{\hbar}{\pi^2} \int_0^\infty \omega d\omega \left[ \frac{1}{e^{\frac{\hbar\omega}{k_B T_c}} - 1} - \frac{1}{e^{\frac{\hbar\omega}{k_B T_{env}}} - 1} \right] \\ \sum_{P=M, N} \sum_{n=-\infty}^{\infty} \int_{-\omega/c}^{\omega/c} dk_z (\text{Re}[T_{n, k_z}^{PP}] + |T_{n, k_z}^{PP}|^2 + |T_{n, k_z}^{P\bar{P}}|^2).$$
 (21)

Obviously, if  $T_c < T_{env}$ , there is a net energy flux into the cylinder. In the following, we consider exclusively the case  $T_{env} = 0$  (and denote  $T_c = T$ ), for which case the

energy flux is referred to as heat radiation of the cylinder. The expression (21) can be split into two terms each representing a different polarization of the corresponding electric field. Specifically, the term which describes polarization parallel to the cylinder is given by the  $N$ -modes,

$$\frac{|H_N|}{L} = \frac{|H_{\parallel}|}{L} = -\frac{\hbar}{\pi^2} \int_0^{\infty} \frac{\omega d\omega}{e^{\frac{\hbar\omega}{k_B T}} - 1} \sum_{n=-\infty}^{\infty} \int_{-\omega/c}^{\omega/c} dk_z (\text{Re}[T_{n,k_z}^{NN}] + |T_{n,k_z}^{NN}|^2 + |T_{n,k_z}^{NM}|^2), \quad (22)$$

whereas the term responsible for the polarization perpendicular to the cylindrical axis is given by the  $M$ -modes,

$$\frac{|H_M|}{L} = \frac{|H_{\perp}|}{L} = -\frac{\hbar}{\pi^2} \int_0^{\infty} \frac{\omega d\omega}{e^{\frac{\hbar\omega}{k_B T}} - 1} \sum_{n=-\infty}^{\infty} \int_{-\omega/c}^{\omega/c} dk_z (\text{Re}[T_{n,k_z}^{MM}] + |T_{n,k_z}^{MM}|^2 + |T_{n,k_z}^{MN}|^2). \quad (23)$$

In the following we use a standard definition of the degree of polarization  $I$  in order to quantify polarization effects,

$$I = \frac{|H_N| - |H_M|}{|H_N| + |H_M|}. \quad (24)$$

In case one prefers a description in terms of the scattering matrix  $\mathbb{S}$  [24, 38] with  $\mathcal{S}_{n,k_z}^{P'P} = 2T_{n,k_z}^{P'P} + \delta_{P,P'}$ , the radiation in Eq. (21) can equivalently be written

$$\frac{|H_c|}{L} = -\frac{\hbar}{4\pi^2} \int_0^{\infty} \omega d\omega \left[ \frac{1}{e^{\frac{\hbar\omega}{k_B T_c}} - 1} - \frac{1}{e^{\frac{\hbar\omega}{k_B T_{env}}} - 1} \right] \sum_{P,P'} \sum_{n=-\infty}^{\infty} \int_{-\omega/c}^{\omega/c} dk_z (|\mathcal{S}_{n,k_z}^{PP'}|^2 - \delta_{P,P'}). \quad (25)$$

Furthermore we note that the result for the perpendicular emission of the cylinder given in Ref. [24] can be recovered from Eq. (21) by restricting to  $k_z = 0$ , taking into account waves normal to the cylindrical axis only. In this case the  $\mathbb{T}$  operator is diagonal in polarization  $P$ .

### C. Limit of large radius (radiation of a plate of anisotropic material)

For large radius, the radiation of a cylinder is asymptotically identical to the radiation of a plate (a semi-infinite planar object) of same surface area [28]. For the case of a plate made of isotropic material, the heat radiation is well-known [36]. Nevertheless, we will below study the heat radiation of a cylinder made of uniaxial material (as a simple model for carbon nanotubes), see Fig. 1, in which case the limit of large radius is a plate of uniaxial material. Recent literature discusses heat transfer between plates of uniaxial materials [41] as well as

Casimir forces between a uniaxial plate and single-walled carbon nanotubes [42], but we have not come across an explicit result for radiation of a plate. For materials with anisotropic electric or magnetic response, the Fresnel coefficients are not diagonal in polarization  $s$  and  $p$  (see Ref. [43] for these lengthy coefficients), but take the general form  $r^{Q'Q}$  for a scattered wave of polarization  $Q'$  in response to an incoming wave of polarization  $Q$ . Note,  $s(p)$  polarization corresponds to the wave with the electric field vector perpendicular (parallel) to the plane of incidence. Thus, the heat radiated per surface area (the Poynting vector  $S$ ) can in this general case easily be found from Eq. (14), where, using a plane-waves basis [40], the steps are similar to the ones performed for the cylinder (Eqs. (16)-(18)).

$$S = \frac{\hbar}{8\pi^3} \int_0^{\infty} d\omega \frac{\omega}{e^{\frac{\hbar\omega}{k_B T}} - 1} \int_{k_{\perp} < \omega/c} d^2 k_{\perp} \sum_{Q=\{s,p\}} \left[ 1 - (|r^Q|^2 + |r^{Q\bar{Q}}|^2) \right], \quad (26)$$

Here,  $k_{\perp}$  is the wave-vector component parallel to the plate. For  $r^{Q\bar{Q}} = 0$ , this equation reduces to the well-known one for isotropic materials [36]. The expression (26) can be rewritten in terms of  $M$  and  $N$  polarization for cylindrical geometry. If we define  $\phi$  to be the angle between the optical axis (which, in order to describe the radiation of a thick cylinder in terms of the one of a plate, is parallel to the plate surface) and the intersection line between the plane of incidence and plate itself, then we can write the limiting values of the  $M$  and  $N$  components of the cylinder radiation as,

$$S_M = \frac{\hbar}{8\pi^3} \int_0^{\infty} d\omega \frac{\omega}{e^{\frac{\hbar\omega}{k_B T}} - 1} \int_0^{2\pi} d\phi \int_0^{\omega/c} k_{\perp} dk_{\perp} \times \left[ 1 - \frac{1}{2} \{ (|r^s|^2 + |r^{sp}|^2) \cos^2 \phi + (|r^p|^2 + |r^{ps}|^2) \sin^2 \phi \} \right]. \quad (27)$$

$$S_N = \frac{\hbar}{8\pi^3} \int_0^{\infty} d\omega \frac{\omega}{e^{\frac{\hbar\omega}{k_B T}} - 1} \int_0^{2\pi} d\phi \int_0^{\omega/c} k_{\perp} dk_{\perp} \times \left[ 1 - \frac{1}{2} \{ (|r^s|^2 + |r^{sp}|^2) \sin^2 \phi + (|r^p|^2 + |r^{ps}|^2) \cos^2 \phi \} \right]. \quad (28)$$

Note  $r^{sp} = r^{ps}$  when the optical axis is parallel to the plate.

### III. $\mathbb{T}$ OPERATOR FOR A CYLINDER MADE OF UNIAXIAL MATERIAL

In section II B, we derived the heat radiation of a cylindrical object expressed in terms of its  $\mathbb{T}$  operator which is known analytically [11, 44]. One aim of this paper is

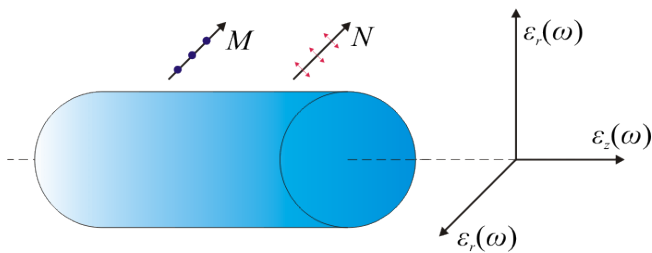


FIG. 1: (color online) Infinitely long cylinder made of a uniaxial material. The symmetry axis of the cylinder coincides with the symmetry axis of the diagonal dielectric tensor (the  $z$ -axis). Electromagnetic waves radiated by the cylinder are denoted by  $M$  and  $N$  for  $M$ -polarized (perpendicular) and  $N$ -polarized (parallel) respectively. Note, generally  $M$ -polarized waves have components along both azimuthal and radial directions. Also, despite  $N$ -polarized waves have non-zero components along all three basis directions, it is only the component parallel to the cylindrical axis to contribute to the Poynting vector.

to study the radiation of a cylinder of uniaxial material as a simple model for carbon nanotubes (see Sec. IV C). The corresponding  $\mathbb{T}$  operator, which seems unavailable in the literature, will be derived here for the case depicted in Fig.1, where the cylindrical axis coincides with the optical axis. This is done by solving the scattering problem in Eq. (10), which amounts to satisfying the boundary conditions for the electromagnetic field at the cylinder's surface. The setup is described by isotropic local magnetic permeability  $\mu(\omega)$  and the following tensor for the anisotropic, but homogeneous and local dielectric function inside the cylinder,

$$\hat{\epsilon}(\omega) = \begin{pmatrix} \epsilon_r(\omega) & 0 & 0 \\ 0 & \epsilon_r(\omega) & 0 \\ 0 & 0 & \epsilon_z(\omega) \end{pmatrix}. \quad (29)$$

The electric displacement field inside the cylinder can then be written as

$$\mathbf{D} = \epsilon_r(\omega) (E_r \mathbf{e}_r + E_\phi \mathbf{e}_\phi) + \epsilon_z(\omega) E_z \mathbf{e}_z,$$

where  $\mathbf{e}_r$ ,  $\mathbf{e}_\phi$  and  $\mathbf{e}_z$  correspond to unit vectors in cylindrical coordinates.

Importantly, uniaxial materials split the incident beam into ordinary and extraordinary ones [45]. In our geometry, cylindrical  $M$ -polarized waves correspond to ordinary ones and propagate according to the dielectric function  $\epsilon_r$ . The  $N$  modes correspond to extraordinary waves and propagate according to an effective dielectric function which depends on the direction of propagation.

The resulting  $\mathbb{T}$  operator components  $T_{n,k_z}^{P'P}$ , as defined in Eq. (15), are expressed in terms of Bessel functions,  $J_n$ , and Hankel functions of first kind,  $H_n^{(1)}$  (see App. B for the detailed derivation),

$$T_{n,k_z}^{MM} = -\frac{J_n(qR)}{H_n^{(1)}(qR)} \frac{\Delta_1 \Delta_4 - K^2}{\Delta_1 \Delta_2 - K^2}, \quad (30)$$

$$T_{n,k_z}^{NN} = -\frac{J_n(qR)}{H_n^{(1)}(qR)} \frac{\Delta_2 \Delta_3 - K^2}{\Delta_1 \Delta_2 - K^2}, \quad (31)$$

$$T_{n,k_z}^{NM} = T_{n,k_z}^{MN} = \frac{2i}{\pi \sqrt{\epsilon_z \mu} (qR)^2} \frac{K}{[H_n^{(1)}(qR)]^2} \frac{1}{\Delta_1 \Delta_2 - K^2}, \quad (32)$$

where

$$\Delta_1 = \frac{J'_n(q_N R)}{q_N R J_n(q_N R)} - \frac{1}{\epsilon_z} \frac{H_n^{(1)'}(qR)}{qR H_n^{(1)}(qR)}, \quad (33)$$

$$\Delta_2 = \frac{J'_n(q_M R)}{q_M R J_n(q_M R)} - \frac{1}{\mu} \frac{H_n^{(1)'}(qR)}{qR H_n^{(1)}(qR)}, \quad (34)$$

$$\Delta_3 = \frac{J'_n(q_N R)}{q_N R J_n(q_N R)} - \frac{1}{\epsilon_z} \frac{J'_n(qR)}{qR J_n(qR)}, \quad (35)$$

$$\Delta_4 = \frac{J'_n(q_M R)}{q_M R J_n(q_M R)} - \frac{1}{\mu} \frac{J'_n(qR)}{qR J_n(qR)}, \quad (36)$$

and

$$K = \frac{nk_z c}{\sqrt{\epsilon_z \mu} R^2 \omega} \left( \frac{1}{q_M^2} - \frac{1}{q^2} \right). \quad (37)$$

$k = \omega/c$  and  $q = \sqrt{k^2 - k_z^2}$  are the wave-vector magnitude in vacuum and its component perpendicular to the  $z$ -axis respectively.  $q_M = \sqrt{\epsilon_r \mu k^2 - k_z^2}$  and  $q_N = \sqrt{\epsilon_z / \epsilon_r} \sqrt{\epsilon_r \mu k^2 - k_z^2}$  are the wave-vector components perpendicular to the  $z$ -axis for the  $M$ -polarized ordinary and  $N$ -polarized extraordinary waves inside the cylinder respectively.

As required by continuity, the above  $\mathbb{T}$  matrix can be easily reduced to the isotropic case when  $\epsilon_r = \epsilon_z = \epsilon$ . Then the expressions simplify to  $q_M = q_N = \sqrt{\epsilon \mu k^2 - k_z^2} \equiv q'$  and  $K = nk_z c (1/q'^2 - 1/q^2) / (\sqrt{\epsilon \mu} R^2 \omega)$ , and our results reduce to the known forms for an isotropic cylinder [11, 44].

#### IV. EXAMPLES AND ASYMPTOTIC RESULTS

In this section we numerically, and analytically, study the radiation of a cylinder for different material classes. We start with isotropic dielectrics and conductors and finally present the case of a uniaxial material using the “in-layer” and “inter-layer” response of graphite to model MWCNT. We consider  $\mu = 1$  for all studied materials.

##### A. Dielectric cylinder

Figure 2 illustrates the result of the numerical calculation of the radiation by  $\text{SiO}_2$  and  $\text{SiC}$  cylinders for

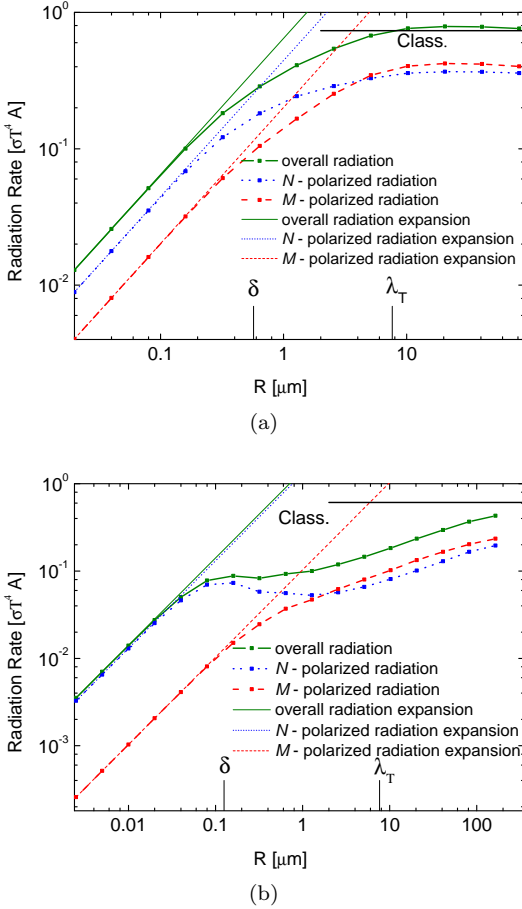


FIG. 2: (color online) The normalized heat radiation as a function of radius  $R$  for (a)  $\text{SiO}_2$  and (b)  $\text{SiC}$  cylinders at temperature  $T = 300\text{K}$ . Calculations were performed using Eq. (21), and analytical expansions, Eq. (38) and Eq. (39). The horizontal lines show the radiation of (a)  $\text{SiO}_2$  and (b)  $\text{SiC}$  plates.  $\lambda_T$  and the smallest skin depths  $\delta$  in the relevant frequency range are marked on  $R$ -axis.

$T = 300\text{K}$  normalized by the Stefan-Boltzmann value, Eq. (2).

For  $\text{SiO}_2$  optical data was used, whereas for  $\text{SiC}$  the following dielectric function was taken [46],

$$\varepsilon_{\text{SiC}}(\omega) = \varepsilon_\infty \frac{\omega^2 - \omega_{LO}^2 + i\omega\gamma}{\omega^2 - \omega_{TO}^2 + i\omega\gamma},$$

where  $\varepsilon_\infty = 6.7$ ,  $\omega_{LO} = 0.12\text{eV}$ ,  $\omega_{TO} = 0.098\text{eV}$ ,  $\gamma = 5.88 \times 10^{-4}\text{eV}$ .

We see the effects discussed in Ref. [28] involving the three length scales: radius  $R$ , thermal wavelength  $\lambda_T$ , and skin depth  $\delta = c/(\text{Im}\sqrt{\varepsilon}\omega)$ , where the latter depends on frequency. If  $R$  is the smallest scale, i.e., much smaller than the smallest *relevant skin depth* and  $\lambda_T$ , the radiation is proportional to the volume of the cylinder. In this case, radiation emitted inside the cylinder will hardly be reabsorbed on its way out so that all regions of the cylinder contribute equally to the emission. The

other asymptotic behavior is approached when  $R$  is the largest scale, i.e. much larger than the largest *relevant skin depth* and  $\lambda_T$ . Then only the cylinder surface contributes to the radiation which approaches the values of a plate of equal surface area as seen in the figure.

The length scale  $\lambda_T$  sets (via the Boltzmann factor) the range of relevant wavelengths of emission. Nevertheless, for dielectrics there is a fine structure to this range given by the resonances of the material. In case of  $R \ll \delta$ , the cylinder emits predominantly at the resonance wavelengths of the material, where  $\delta$  is minimal. On the other hand, for  $R \gg \{\delta, \lambda_T\}$ , the emissivity is strongest in regions where  $\varepsilon \approx 1$  (compare the plate emissivity).

In general, one might expect resonance effects when the emitted wavelength is of the order of  $R/(2\pi)$  (similar to Mie resonances for a sphere [11, 12]). Due to the contribution of all wavelengths, these are smeared out in the total heat emitted. For  $\text{SiO}_2$  in Fig. 2, the fact that the emissivity exceeds the plate result for  $R \approx 20\mu\text{m}$  might be connected to such resonances.

Figure 2 shows imprints of the dielectric function of  $\text{SiC}$  which has a sharp strong resonance (leading to a small  $\delta$ ), but apart from the resonance,  $\text{SiC}$  is almost black (i.e. has very large  $\delta$ ) in our frequency range. The two regimes  $R \ll \{\delta, \lambda_T\}$  and  $R \gg \{\delta, \lambda_T\}$ , where the cylinder radiation follows the discussed asymptotic laws are far apart, and very large radii  $R$  are necessary to approach the classical plate result. In Fig. 2, the radiation for  $R = 150\mu\text{m}$  is still distinctly different from the asymptotic result. This might be advantageous for experiments, as a  $\text{SiC}$  cylinder does not have to be very thin in order to observe deviations from the Stefan-Boltzmann law.

In the limit of  $R \ll \{\delta, \lambda_T\}$ , the radiation can be studied analytically, see App. C, where we find the following asymptotic laws for the two polarizations,

$$\lim_{R \ll \{\delta, \lambda_T\}} \frac{|H_N|}{A} = \frac{1}{6} \int_0^\infty \frac{d\omega}{(2\pi)^4} a_T(\omega) cR \times \text{Im} \frac{\varepsilon(\omega)^2 + 2\varepsilon(\omega) - 1}{\varepsilon(\omega) + 1}, \quad (38)$$

$$\lim_{R \ll \{\delta, \lambda_T\}} \frac{|H_M|}{A} = \frac{1}{2} \int_0^\infty \frac{d\omega}{(2\pi)^4} a_T(\omega) cR \text{Im} \frac{\varepsilon(\omega) - 1}{\varepsilon(\omega) + 1}. \quad (39)$$

Note the linear increase with  $R$ , corresponding to the proportionality of the unnormalized radiation to the volume. The numerical evaluation of these asymptotic forms has been added to the graphs in Fig. 2, where the agreement for small  $R$  to the full results is visible. As expected and seen from the equations above, cylinders with purely real dielectric functions (or more general with real potential  $\mathbb{V}$ ) will not radiate, because the dissipative properties of the material are responsible for the heat radiation (in accord with FDT). This holds for any  $R$ . The  $N$ -polarization given in Eq. (38) dominates over the  $M$ -polarization in Eq. (39) if

$$[\text{Re} \varepsilon(\omega) + 1]^2 + [\text{Im} \varepsilon(\omega)]^2 \gg \text{Im} \varepsilon(\omega) \quad (40)$$



holds, which is the case for most materials. Further insight can be gained by additionally requiring the temperature to be so low that one can expand the dielectric function, i.e.,  $\lambda_T \gg \lambda_0$ , where  $\lambda_0$  is the wavelength of the lowest resonance of the material. In this case [39],

$$\varepsilon(\omega) = \varepsilon_0 + i \frac{\lambda_{in}\omega}{c} + \mathcal{O}(\omega^2), \quad (41)$$

with  $\varepsilon_0$  and  $\lambda_{in}$  real. Plugging (41) into Eqs.(38) and (39) the frequency integration can be done and we have,

$$\lim_{R \ll \{\delta, \lambda_T\}, \lambda_0 \ll \lambda_T} \frac{|H_N|}{A} = \frac{4\pi^4 \hbar c^2 \lambda_{in} R}{189 \lambda_T^6} \left[ 1 + \frac{2}{(\varepsilon_0 + 1)^2} \right], \quad (42)$$

$$\lim_{R \ll \{\delta, \lambda_T\}, \lambda_0 \ll \lambda_T} \frac{|H_M|}{A} = \frac{8\pi^4 \hbar c^2 \lambda_{in} R}{63 \lambda_T^6} \frac{1}{(\varepsilon_0 + 1)^2}. \quad (43)$$

Interestingly, to lowest order in  $T$ , both components scale as  $T^6$  and hence fundamentally different from the Stefan-Boltzmann law in Eq. (2), which scales as  $T^4$ .

The degree of polarization  $I$  in Eq. (24) is finally given by

$$\lim_{R \ll \{\delta, \lambda_T\}, \lambda_0 \ll \lambda_T} I = \frac{\varepsilon_0^2 + 2\varepsilon_0 - 3}{\varepsilon_0^2 + 2\varepsilon_0 + 9}. \quad (44)$$

Although the condition  $\lambda_0 \ll \lambda_T$  is not fulfilled in Fig. 2, Eq. (44) still gives a hint to why SiC has higher degree of polarization compared to SiO<sub>2</sub>, as  $\varepsilon_0$  is tangibly larger for SiC and Eq. (44) monotonically increases with  $\varepsilon_0$  (for  $\varepsilon_0 > 0$ ).

## B. Well conducting cylinder

Conductors differ from insulators by a significantly smaller skin depth  $\delta$ , leading to very different radiation characteristics. In this section, we first study the radiation using a simple Drude model with the parameters of gold in order to highlight the different limiting behaviors. Then, we turn to tungsten which has been extensively used in experiments[16, 24].

The Drude model for gold[47],

$$\varepsilon_{Au}(\omega) = \varepsilon_\infty - \frac{\omega_p^2}{\omega(\omega + i\omega_\tau)}, \quad (45)$$

has the parameters  $\varepsilon_\infty = 1$ ,  $\omega_p = 9.03eV$  and  $\omega_\tau = 2.67 \times 10^{-2}eV$ .

Figure 3 shows the numerical result for the total radiation by a gold cylinder at 300K and 30K. We observe a behavior drastically different from the ones in Fig. 2: the radiation, normalized by surface area, can be many orders larger than expected from the Stefan-Boltzmann law. More precisely, it increases with decreasing  $R$ , has a maximum at  $R \approx \delta$  (for Drude model of gold (45),  $\delta(\omega)$  has no sharp minimum, and we show the skin depth

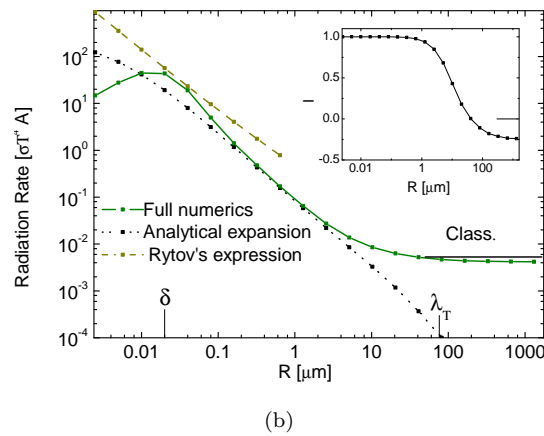
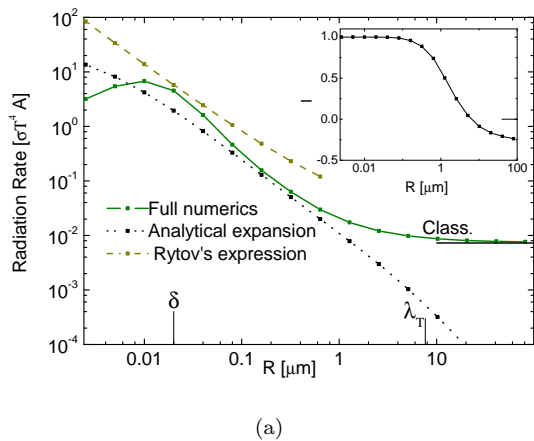
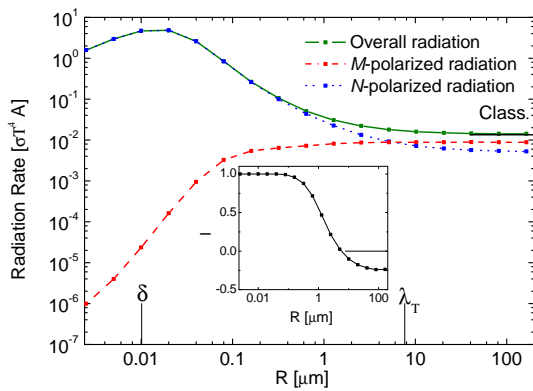


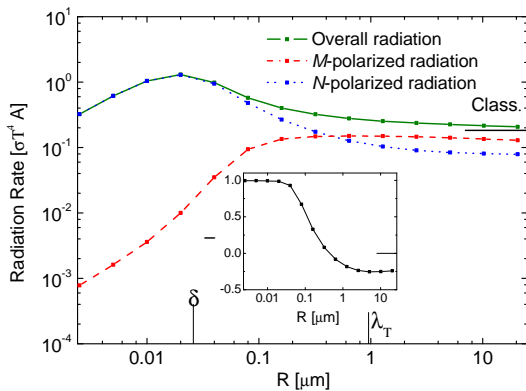
FIG. 3: (color online) The normalized heat radiation as a function of radius  $R$  for Au cylinder at temperatures (a)  $T = 300K$  and (b)  $T = 30K$ . Calculations were performed using the Drude model [47] with Au optical properties. Full numerics, Eq. (21), analytical expansion, Eq. (46), and the approximation of Eq. (47) were used. Black horizontal lines indicate the radiation of Au plates at corresponding temperatures.  $\lambda_T$  and the skin depth  $\delta$  in the relevant frequency range are marked on the  $R$ -axis. In the insets the degree of polarizations, (24), are plotted.

corresponding roughly to thermal wavelength) and approaches the laws (38) and (39) only for very small (unphysical) radii. For  $R \gg \lambda_T$ , the result of a gold plate is approached. The large values of radiated power, compared to the Stefan-Boltzmann law, can be explained by the interplay of two effects: a large imaginary part of the dielectric function gives rise to strong radiation from every volume element of the conductor. On the other hand, it also leads to a very small skin depth such that most radiation is reabsorbed inside the conductor, and only a thin surface layer contributes to the radiation. In the region where  $R \approx \delta$ , one has very strong emitting elements which all contribute to the total radiation, and hence emission normalized by surface area is maximal. Interestingly, when the conductivity goes to infinity, the effect of vanishing skin depth is stronger than the effect





(a)



(b)

FIG. 4: (color online) The normalized heat radiation as a function of radius  $R$  for tungsten cylinder at temperatures (a)  $T = 298K$  and (b)  $T = 2400K$ . Calculations were performed using Eq.(21) with dielectric function (48). Black horizontal lines indicate the radiation of tungsten plates at corresponding temperatures.  $\lambda_T$  and the skin depth  $\delta$  in the relevant frequency range are marked on  $R$ -axis. In the insets the degree of polarizations are given using expression (24).

of increasing radiation such that the emissivity vanishes as  $1/\sqrt{\epsilon}$ . In this case, the classical (plate) limit goes to zero and the maximum in the curve shifts to smaller and smaller  $R$ .

The insets show the degree of polarization (24) as a function of  $R$ . For  $R \lesssim \lambda_T$ , the radiation from the gold cylinder is fully  $N$ -polarized. For  $R \gtrsim \lambda_T$ , the degree of polarization becomes negative and asymptotically approaches zero for  $R/\lambda_T \rightarrow \infty$ . These qualitative features agree with experimental[16–19, 24] as well as theoretical[24] studies on radiation of thin wires.

For conductors, the appropriate limit for an analytic expansion is  $\lambda_T \gg R \gg \delta$  (where  $\delta$  is of the order of nanometers for good conductors). In this case, the leading element of the  $\mathbb{T}$  operator is  $T_{0,k_z}^{NN}$ , see App. D. The resulting radiation is then completely  $N$ -polarized and reads

$$\lim_{\lambda_T \gg R \gg \delta} \frac{|H_c|}{A} = \int_0^\infty \frac{d\omega}{(2\pi)^2} a_T(\omega) \frac{c^2}{(2\pi)^2 \omega} \int_0^{\pi/2} d\theta \frac{2\text{Re}[1/\sqrt{\epsilon}] \cos^3 \theta}{|\cos^2 \theta (2\gamma_E - i\pi)\omega R/c - 2i/\sqrt{\epsilon} + 2 \cos^2 \theta \omega R/c \log[\cos \theta \omega R/2c]|^2}, \quad (46)$$

where  $\gamma_E \approx 0.577$  is Euler-Mascheroni constant and  $\theta$  is the angle of incidence so that  $k_z = k \sin \theta$ .

As described above, we see here explicitly that the radiation (in the considered range of radii) vanishes for  $|\epsilon| \rightarrow \infty$ . This expression cannot be further simplified as the integrand diverges at  $\theta = \pi/2$  if we omit the small term  $-2i/\sqrt{\epsilon}$  in the denominator. A result almost similar to (46) was obtained by Rytov [48] (whose derivation was restricted to  $\text{Re}\epsilon = 0$  and  $\text{Im}\epsilon \gg 0$ ), which differs by the absence of the first term in denominator. We em-

phasize however that this term is necessary for accurate results in the considered limit.

Rytov suggests a further simplification of his expression by setting  $\cos \theta = 1$  in  $\log[\cos \theta \omega R/2c]$ , so that integration can be performed analytically. Omitting  $\cos^2 \theta (2\gamma_E - i\pi)\omega R/c$  in denominator, the following result

for radiation can be obtained after integration,

$$\lim_{\lambda_T \gg R \gg \delta} \frac{|H_c|}{A} \approx \int_0^\infty \frac{d\omega}{(2\pi)^2} \frac{c^{7/2}}{2(2\pi)^2 \omega^{5/2}} \times a_T(\omega) \text{Re}[1/\sqrt{\varepsilon}] \frac{|\varepsilon|^{1/4}}{|R \log[\omega R/2c]|^{3/2}}. \quad (47)$$

Note that Eq. (47) was derived for any well-conducting (non magnetic) media, whereas the corresponding result, Eq. (IV.35) in Ref. [48], only considers the case of a purely imaginary dielectric function (and  $\mu \neq 1$ ). Due to this the integrand of Eq. (47) differs from Eq. (IV.35) in Ref. [48] by  $\text{Re}[1/\sqrt{\varepsilon}]|\varepsilon|^{1/4}$  instead of  $(\mu/4 \text{Im} \varepsilon)^{1/4}$  (which agree for  $\text{Re} \varepsilon = 0$  and  $\mu = 1$ ). Also, we emphasize that Eq. (47) is an approximation whereas Eq. (46) is exact asymptotic limit for  $\lambda_T \gg R \gg \delta$ .

Figure 3 provides a test of these approximations, demonstrating that for  $T = 30K$ , where the ratio of  $\lambda_T$  and  $\delta$  is larger than at  $T = 300K$ , Eq. (46) describes the full solution over roughly one decade in  $R$ . For  $T = 300K$ , the agreement is not as good as the ratio of  $\lambda_T$  and  $\delta$  is too small. Equation (47) gives a rough estimate of the overall dependence on  $R$  in Fig. 3, but the values differ by roughly a factor of 10 from the exact results. Moreover, above some threshold value of  $R$  we cannot obtain a finite radiation rate from Eq. (47) because of the divergent term due to log of unity in the denominator of the integrand.

After this (more theoretical) discussion of gold, where we used the same  $\varepsilon$  for both temperatures in order to demonstrate the pure effect of temperature via the Boltzmann factor, we turn to the experimentally relevant material tungsten, at relevant temperatures of  $T = 298K$  and  $T = 2400K$  as shown in Fig. 4. We use the corresponding dielectric function for tungsten[49],

$$\varepsilon_W(\omega) = 1 + \sum_{p=1}^3 \frac{K_{0p} \lambda^2}{\lambda^2 - \lambda_{sp}^2 + i\delta_p \lambda_{sp} \lambda} - \frac{\lambda^2}{2\pi c \varepsilon_0} \sum_{q=1}^2 \frac{\sigma_q}{\lambda_{rq} - i\lambda}, \quad (48)$$

where  $\lambda$  is the wavelength in vacuum,  $c$  is the velocity of light and  $\varepsilon_0$  is the permittivity of vacuum in SI units. The remaining parameters are listed in Table I.

The overall radiation of tungsten at  $298K$  is very similar to gold at  $300K$  in Fig. 3. At high temperature  $T = 2400K$ , the increase of the normalized radiation over the Stefan-Boltzmann law is reduced. We attribute this to a smaller conductivity at  $T = 2400K$ . We also observe in the insets that the zero in the polarization curves shifts by roughly a factor of 10 when comparing the two temperatures. This manifests that the zero in the polarization curves is mostly a function of  $R/\lambda_T$  as  $\lambda_T$  is also shifted by almost a factor of 10. Furthermore, although the polarization in the inset is indistinguishable from unity at small  $R$ , we note that the ratio of  $N$  and  $M$  polarizations is a factor of  $10^3$  larger for  $T = 298K$  compared to  $T = 2400K$ .

$T$	298	2400
$\sigma_1$	17.5	1.19
$\sigma_2$	0.21	0.25
$\lambda_{r1}$	45.5	3.66
$\lambda_{r2}$	3.7	0.36
$K_{01}$	12	
$K_{02}$	14.4	
$K_{03}$	12.9	
$\lambda_{s1}$	1.26	
$\lambda_{s2}$	0.6	
$\lambda_{s3}$	0.3	
$\delta_1$	0.6	
$\delta_2$	0.8	
$\delta_3$	0.6	

TABLE I: Optical data for tungsten from [49]. Temperature  $T$  is in Kelvins. Conductivities ( $\sigma_1$ , etc.) are in units of  $10^6 \text{ ohm}^{-1} \text{ m}^{-1}$ . Wavelengths ( $\lambda_{r1}$ , etc.) are in  $\mu\text{m}$ .  $K_{01}$ , etc. and  $\delta_1$ , etc. are dimensionless.

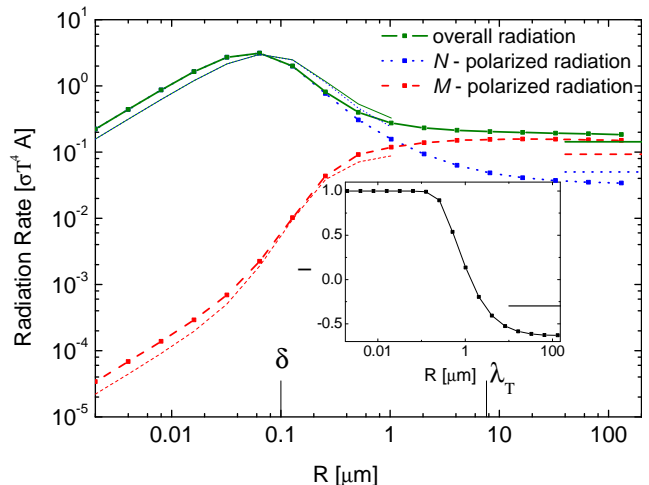


FIG. 5: (color online) The heat radiation of a MWCNT as a function of radius  $R$ , normalized by the Stefan-Boltzmann result, at  $T = 300K$ . Contributions from two polarizations are indicated. Corresponding thin curves without boxes represent the heat radiation for “isotropic graphite” with dielectric function  $(\varepsilon_z + \varepsilon_r)/2$ . Horizontal lines of different colors indicate the graphite plate classical result for correspondingly colored curves.  $\lambda_T$  and the smallest skin depth  $\delta$  in the relevant frequency range are marked on the  $R$ -axis. Note that the smallest skin depths corresponding to both  $\varepsilon_r$  and  $\varepsilon_z$  are approximately equal and labeled here by  $\delta$ . In the inset the degree of polarization is given using expression (24).

### C. Multi-walled carbon nanotube

We finally turn to heat radiation of a cylinder made of uniaxial material. This can be considered a simple model for a MWCNT[50] which is of high importance in modern science and technology. As a MWCNT is a wrapped up

$j$	1	2	3	4	5	6	7
$f_j$	0.134	0.072	0.307	0.380	0.065	0.553	1.381
$\alpha_j$	24.708	0.524	0.217	0.518	0.286	0.248	15.101
$\omega_{tj}$	2.358	5.149	13.785	10.947	16.988	24.038	36.252
$\Gamma_j$	9.806	472.7	4.651	1.797	2.418	21.395	37.025

TABLE II: Optical parameters for the in-layer dielectric function of graphite ( $\varepsilon_z$ ) from [51].  $f_j$  and  $\alpha_j$  are dimensionless, whereas  $\omega_{tj}$  and  $\Gamma_j$  are in  $eV$ .

$j$	1	2	3	4	5	6	7
$f_j$	0.073	0.056	0.069	0.005	0.262	0.460	0.200
$\alpha_j$	0.505	7.079	0.362	7.426	0.000382	1.387	28.963
$\omega_{tj}$	0.275	3.508	4.451	13.591	14.226	15.550	32.011
$\Gamma_j$	4.102	7.328	1.414	0.046	1.862	11.922	39.091

TABLE III: Optical parameters for the inter-layer dielectric function of graphite ( $\varepsilon_r$ ) from [51].  $f_j$  and  $\alpha_j$  are dimensionless, whereas  $\omega_{tj}$  and  $\Gamma_j$  are in  $eV$ .

graphite sheet, we can in a crude approximation regard it as a (solid) cylinder described by two different dielectric response functions: the response along the cylindrical axis is given by the in-layer properties of the graphite sheets, whereas the response perpendicular to this axis is approximately given by the inter-layer response. We also note that most mineral crystals have uniaxial optical properties, and heat emission by these materials might open new possibilities for applications[41].

Figure 5 shows the heat radiation of a MWCNT for  $T = 300K$  using expressions (21) and (30)-(37), normalized as before by the Stefan-Boltzmann law  $H = \sigma T^4 A$ . We used the following form for the graphite dielectric function[51],

$$\varepsilon_{r,z}(\omega) = 1 - \frac{\Omega_p^2}{\omega(\omega + i\Gamma_0)} - \sum_j \frac{f_j \omega_p^2}{(\omega^2 - \omega_{tj}^2) + i\omega\Gamma'_j}, \quad (49)$$

where  $\Omega_p = \sqrt{f_0}\omega_p$  and a specific form of  $\Gamma'_j = \Gamma_j \exp\left[-\alpha_j \left(\frac{\hbar\omega - \hbar\omega_j}{\Gamma_j}\right)^2\right]$  is used, which best describes the experimental data. For the dielectric function component  $\varepsilon_z$  along the cylindrical axis, i.e., the in-layer response, the parameters are  $\omega_p = 19eV$ ,  $\Gamma_0 = 0.091eV$ ,  $f_0 = 0.016$ . The remaining parameters are given in Table II. For the dielectric function component  $\varepsilon_r$  perpendicular to the cylindrical axis, i.e., the inter-layer response, the parameters are  $\omega_p = 27eV$ ,  $\Gamma_0 = 6.365eV$ ,  $f_0 = 0.014$  and the remaining parameters are given in Table III.

These parameterizations apply to the frequency range  $0.12 - 40eV$  and  $2 - 40eV$  for  $\varepsilon_r$  and  $\varepsilon_z$  respectively, but we nevertheless use them for the range of roughly  $0.004 - 0.2eV$  due to the lack of simple analytic forms for the broader range. Note that  $\lambda_T$  corresponds to a frequency of  $0.163eV$  for  $T = 300K$ .

The overall radiation curve is in between the characteristic shapes of dielectrics and conductors (compare Figs 2

and 3): the regime proportional to volume as in Eqs. (38) and (39) is visible for small  $R$  in contrast to Fig. 3. On the other hand, the strong increase over the plate-result and over the Stefan-Boltzmann value, characteristic for conductors, is visible as well. These features follow from the dielectric functions in Eq.(49) carrying a smaller conductivity compared to gold.

In order to highlight the effect of material anisotropy, in Fig. 5 we also show the thin curves without boxes for which we use an isotropic dielectric function, given by  $(\varepsilon_z + \varepsilon_r)/2$ . We see that the influence of anisotropy on the radiation is almost negligible at small  $R$ , whereas at intermediate  $R$  it strongly increases the degree of polarization perpendicular to the tube. Interestingly, the asymptotic value of  $I$  in the inset is different from 0 and takes the value  $-0.297$ , an effect purely due to the anisotropy which is computed using the result for a plate of anisotropic material, Eqs.(27) and (28). We note that a very thick MWCNT might in fact be best described by a plate with optical axis *perpendicular* to the surface. Thus, while Fig. 5 gives the correct radiation for a material with the dielectric properties given in Eq. (49), it probably only describes MWCNT for small  $R$ . Since, at small  $R$ , the polarization is hardly dependent on the anisotropy of the material, we conclude that the polarization effects for MWCNT [21] are mainly an effect of cylindrical geometry rather than anisotropy of the material.

## V. SPECTRAL EMISSIVITY

In Sec. IV, we studied the total heat radiation of a cylinder made of different materials. While this is of interest in connection with efficient heating or cooling, another quantity which can be more appropriate for direct comparison to experiments is the spectral emissivity. In this section, we discuss the spectral emissivity for cylinders made of dielectrics ( $\text{SiO}_2$ ), conductors (tungsten) and uniaxial materials (graphite) for a fixed radius of  $R = 5\mu\text{m}$ .

The spectral emissivity (density)  $H_\omega$  is given by the integrand of Eq. (21),

$$\frac{|H_\omega|}{L} = -a_T(\omega) \frac{c^4}{(2\pi)^4 \omega^3} \sum_{P=M,N} \sum_{n=-\infty}^{\infty} \int_{-\omega/c}^{\omega/c} dk_z (\text{Re}[T_{n,k_z}^{PP}] + |T_{n,k_z}^{PP}|^2 + |T_{n,k_z}^{P\bar{P}}|^2). \quad (50)$$

We denote by  $H_{\omega M}$  and  $H_{\omega N}$  the correspondingly polarized components of  $H_\omega$ .

### A. SiO<sub>2</sub>

Figure 6 illustrates the spectral density for  $\text{SiO}_2$  at  $T = 300K$ . The unsteady local fine structure reflects

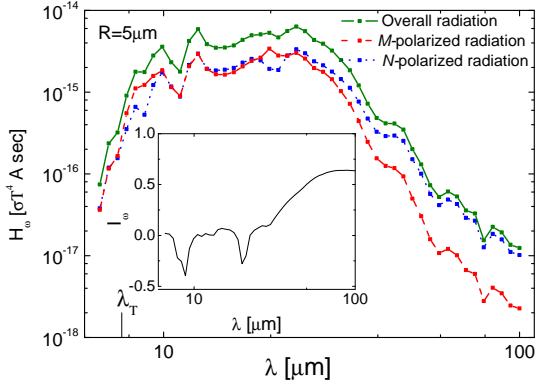


FIG. 6: (color online) The spectral density divided by Stefan-Boltzmann law as a function of wavelength  $\lambda$  for  $\text{SiO}_2$  cylinder of radius  $R = 5\mu\text{m}$  at temperature  $T = 300\text{K}$ . In the inset the spectral degree of polarization is provided.

the nature of the optical data which has a number of smaller peaks. For short wavelengths (high frequencies)  $M$ -polarized radiation mostly dominates, whereas for  $\lambda \gtrsim 25\mu\text{m}$  the  $N$ -polarized radiation starts to prevail up to the limit of long wavelengths (low frequencies). In the inset the spectral degree of polarization as a function of wavelength is shown, where

$$I_\omega = \frac{|H_{\omega N}| - |H_{\omega M}|}{|H_{\omega N}| + |H_{\omega M}|}. \quad (51)$$

The two large valleys in this curve are due to the two dominant resonances of  $\text{SiO}_2$ . The fact that the resonances lead to negative valleys in the polarization is a feature specific for the radius chosen. For large wavelengths, the spectral degree of polarization approaches a constant value, which can be computed easily using expressions (38) and (39),

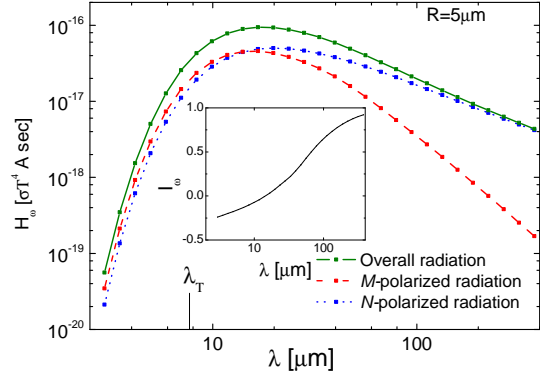
$$\lim_{\{\delta, R\} \ll \lambda} I_\omega = \frac{|\varepsilon(\omega)|^2 + 2 \text{Re} \varepsilon(\omega) - 3}{|\varepsilon(\omega)|^2 + 2 \text{Re} \varepsilon(\omega) + 9}. \quad (52)$$

Furthermore, if additionally  $\lambda \gg \lambda_0$  holds, the dielectric function is described by Eq.(41) and the spectral degree of polarization is given then by Eq.(44).

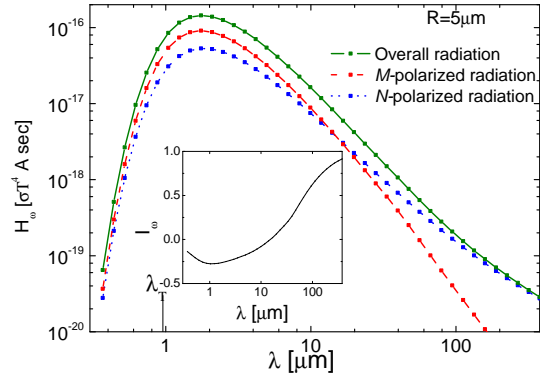
Note that the spectral degree of polarization is independent of temperature if the dielectric function is independent of temperature.

## B. Tungsten

Figure 7 shows the spectral density of radiation for tungsten cylinders at  $T = 298\text{K}$  and  $T = 2400\text{K}$ . The shape of the curves is very similar to Planck's classical law due to the Bose-Einstein statistics factor in  $a_T(\omega)$ . The curves peak at values slightly larger than the corresponding thermal wavelengths. For short wavelengths  $M$ -polarized radiation is stronger than  $N$ -polarized one,



(a)



(b)

FIG. 7: (color online) The spectral density divided by Stefan-Boltzmann law as a function of wavelength  $\lambda$  for tungsten cylinder of radius  $R = 5\mu\text{m}$  at temperatures (a)  $T = 298\text{K}$  and (b)  $T = 2400\text{K}$ . In the insets the spectral degrees of polarization are provided.

whereas for  $\lambda \gtrsim 2R$ ,  $N$ -polarized radiation dominates, strongly suppressing the  $M$ -polarized radiation in the limit of long wavelengths. This transition of polarization is also manifested in the insets where spectral degrees of polarizations are plotted. In the limit of long wavelengths these approach unity, as can be justified by results of Sec.IV B, where it is shown that the  $N$  component is dominant in the limit  $\lambda_T \gg R \gg \delta$ . On the other hand, in the limit of short wavelengths the spectral degree of polarization approaches zero as the cylinder radiates as an isotropic plate. We emphasize again that the spectral degree of polarization is independent of temperature (if  $\varepsilon(\omega)$  is).

## C. Graphite

Figure 8 shows corresponding results for a graphite cylinder at  $T = 300\text{K}$ , displaying similar behavior as the case of conductors in Fig.7. The transition point, where

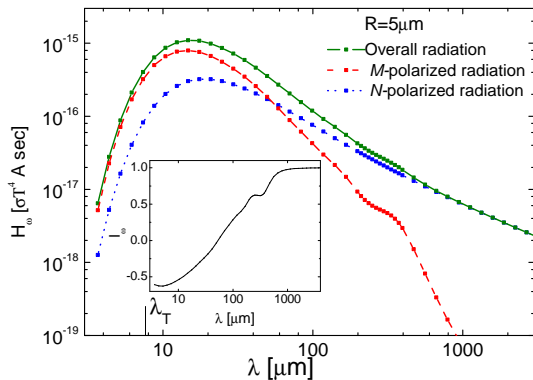


FIG. 8: (color online) The spectral density divided by Stefan-Boltzmann law as a function of wavelength  $\lambda$  for graphite cylinder of radius  $R = 5\mu\text{m}$  at temperature  $T = 300\text{K}$ . In the inset the spectral degree of polarization is provided.

the polarization changes sign is at  $\lambda \approx 25\mu\text{m}$ . Analogously to conductors, the spectral degree of polarization for a graphite cylinder tends to unity in the limit of long wavelengths, i.e. spectral density has polarization parallel to the cylinder. The range of wavelengths  $200-300\mu\text{m}$  shows an unexpected wiggle in the curves, the origin of which is unclear.

We note that  $I_\omega$  goes to zero for  $\lambda \rightarrow 0$ , although a finite value is approached for  $R/\lambda_T \rightarrow \infty$  in Fig. 5. This is due to the fact that both  $\varepsilon_z$  and  $\varepsilon_r$  tend to 1 for  $\omega \rightarrow \infty$ , and the material is asymptotically isotropic. Nevertheless, at  $\lambda \approx 5\mu\text{m}$ , the polarization is very strong compared to Fig. 7, an effect which we attribute to the anisotropy of the material.

Another model describing the spectral degree of polarization of MWCNT's is presented in Ref. [26], where we note partly common structure to our description arising from the expansions of Eqs. (C.1)-(C.5). For large  $\lambda/R \rightarrow \infty$ , both the experimental data as well as the theoretical predictions of Ref. [26] give values for  $I_\omega$  close to unity, in agreement to Fig. 8.

#### D. Comparing material classes

Finally, Fig. 9 compares the spectral polarization for the different materials discussed, where we used simplified dielectric functions for dielectrics and uniaxial materials in order to illuminate the pure influence of  $\lambda/R$ .

Figure 9 manifests that the overall dependence of the polarization on wavelength is quite universal following similar curves for all cases shown. Fundamental differences are seen in the limiting cases. In the limit of large wavelengths all conductors approach unity, whereas dielectrics go to a constant value different from unity when  $\lambda \gg \{\delta, R\}$  (see Eq. (52)).

In the opposite limit of small wavelengths, Fig. 9 manifests strong dependence of the polarization on uniaxiality.

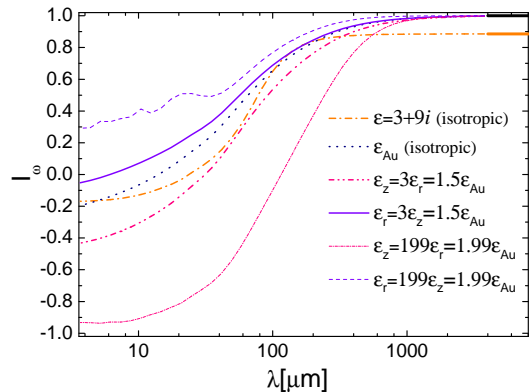


FIG. 9: (color online) Spectral degree of polarization as a function of wavelength  $\lambda$  for cylinders made of isotropic dielectric, isotropic conducting, and anisotropic conducting materials for  $R = 5\mu\text{m}$ . Black horizontal and orange lines correspond to long wavelengths limiting values for conductors (isotropic and uniaxial) and the dielectric (using Eq. (52)), respectively.

We emphasize that by showing additionally artificial materials with very strong anisotropy (factor 199 between  $\varepsilon_r$  and  $\varepsilon_z$ ). Varying this factor, a range from roughly 0.4 to -0.9 in polarization at  $\lambda = 10\mu\text{m}$  can be swept. Figure 9 clearly illustrates that the smaller  $\varepsilon_r/\varepsilon_z$ , the smaller the spectral polarization.

## VI. DISCUSSION

In this article, we derived the general formalism to study the heat radiation of a single object held at uniform temperature. While the presented formalism can describe the radiation of arbitrary objects, we focus on cylindrical objects, providing explicitly the heat radiation formula (Eq. (21)) in terms of its  $\mathbb{T}$  operator. In order to work out the radiation of multi-walled carbon nanotubes in a simple model, we derive the  $\mathbb{T}$  operator for a cylinder made of uniaxial material. We study the cases of dielectrics, conductors and MWCNT numerically, discussing certain limits (e.g. small radius) analytically. To lowest order in temperature  $T$ , the heat emitted by dielectric cylinders is proportional to  $T^6$  in contrast to  $T^4$  in the Stefan-Boltzmann law, Eq. (2).

For all materials, the limiting value of very large radius is given by the radiation of a plate of equal material. In the limit of small radius, dielectrics emit proportional to their volume, whereas this regime is not reached for conductors in the physically relevant range of radii. Instead, the radiation normalized per surface area can be very large for conductors and we observe values as high as almost a hundred times the value expected from the Stefan-Boltzmann law. The maximum occurs where the radius is roughly equal to the skin depth (e.g. a few nm for gold). We note that the validity of using a continuous

dielectric function at the scale of nanometers is questionable and has to be addressed in future studies.

The heat radiated by a long cylinder is polarized. All studied materials show common overall features of their degree of polarization: cylinders with radius smaller than the thermal wavelength emit predominantly radiation polarized parallel to their axis, whereas for radii larger than the thermal wavelength, the polarization points into the direction perpendicular to the cylinder. The limiting value of the degree of polarization for small radii is different for insulators and conductors: while the former approach a value less than unity, thin conductors emit completely polarized radiation and the degree of polarization approaches unity.

The effect of uniaxiality on the polarization is most dominant for large radii, where the degree of polarization can be tuned over a wide range by adjusting the ratio of parallel and perpendicular responses. For small radii, uniaxiality hardly influences the polarization. As MWCNT fall into the latter size regime, we conclude that the polarization measured experimentally for nanotubes are mostly a consequence of geometry, and not so much of material anisotropy.

Detailed comparison to experimental data (see e.g. Refs. [25–27] for MWCNTs) will be left for future work.

### Acknowledgments

We thank T. Emig, R. L. Jaffe, G. Bimonte, M. F. Maghrebi, M. T. H. Reid and N. Graham for helpful discussions. We are especially grateful to T. Emig for providing us with unpublished notes on  $\mathbb{T}$  matrix for an isotropic cylinder and to M. F. Maghrebi for pointing us to the possibility of writing the radiation in the form of Eq. (25). This research was supported by the NSF Grant No. DMR-08-03315, DARPA contract No. S-000354 and the DFG grant No. KR 3844/1-1.

### Appendix A: Cylindrical harmonics and Free Green's function in cylindrical basis

According to Ref. [40], the cylindrical harmonics can be written as,

$$\begin{aligned} \mathbf{RM}_{n,k_z}(\mathbf{r}) &= \left[ \frac{in}{qr} J_n(qr) \mathbf{e}_r - J'_n(qr) \mathbf{e}_\phi \right] e^{ik_z z + in\phi}, \\ \mathbf{RN}_{n,k_z}(\mathbf{r}) &= \frac{c}{\omega} \left[ ik_z J'_n(qr) \mathbf{e}_r - \frac{nk_z}{qr} J_n(qr) \mathbf{e}_\phi \right. \\ &\quad \left. + q J_n(qr) \mathbf{e}_z \right] e^{ik_z z + in\phi}, \end{aligned} \quad (\text{A.1})$$

where  $J_n$  is the Bessel function of order  $n$ .  $\mathbf{RM}_{n,k_z}$  and  $\mathbf{RN}_{n,k_z}$  correspond to regular magnetic multipole (TE) and electric multipole (TM) waves respectively. Also,  $k_z$  and  $q$  are the wavevectors parallel and perpendicular to

the cylindrical  $z$ -axis respectively satisfying the relation  $q = \sqrt{k^2 - k_z^2}$ ,  $k = \omega/c$ .  $J'_n$  corresponds to the first derivative with respect to the argument. Furthermore, we denote the corresponding outgoing waves by  $\mathbf{M}_{n,k_z}$  and  $\mathbf{N}_{n,k_z}$ , which differ from regular ones by replacing  $J_n$  with the Hankel function of the first kind  $H_n^{(1)}$ .

The above solutions correspond to transverse waves, i.e.  $\nabla \cdot \mathbf{RM}_{n,k_z} = \nabla \cdot \mathbf{RN}_{n,k_z} = 0$ . Moreover, they obey useful relations  $\mathbf{RM}_{n,k_z} = \frac{c}{\omega} \nabla \times \mathbf{RN}_{n,k_z}$ ,  $\mathbf{RN}_{n,k_z} = \frac{c}{\omega} \nabla \times \mathbf{RM}_{n,k_z}$ . These relations are also valid for outgoing waves.

The free Green's function in cylindrical waves reads [40],

$$\begin{aligned} \mathbb{G}_0(\mathbf{r}, \mathbf{r}') &= \sum_{P=M,N} \sum_{n=-\infty}^{\infty} (-1)^n \int_{-\infty}^{\infty} \frac{idk_z}{8\pi} \\ &\times \begin{cases} [\mathbf{RM}_{n,k_z}(\mathbf{r}) \otimes \mathbf{P}_{-n,-k_z}(\mathbf{r}')] , & r' > r \\ [\mathbf{P}_{n,k_z}(\mathbf{r}) \otimes \mathbf{RM}_{-n,-k_z}(\mathbf{r}')] , & r' < r. \end{cases} \end{aligned} \quad (\text{A.2})$$

The following relation for propagating cylindrical waves is useful for deriving the Poynting vector,

$$\begin{aligned} \text{Re} \left[ ir \int_0^{2\pi} d\phi \left( \mathbf{RM}_{n,k_z}(\mathbf{r}) \times \nabla \times \mathbf{P}_{n,k_z}^*(\mathbf{r}) T_{n,k_z}^{P'P*} \right. \right. \\ \left. \left. + \mathbf{P}_{n,k_z}(\mathbf{r}) \times \nabla \times \mathbf{RM}_{n,k_z}^*(\mathbf{r}) T_{n,k_z}^{PP'} \right) \cdot \mathbf{e}_r \right] \\ = 4\delta_{P,P'} \text{Re} [T_{n,k_z}^{PP'}], \\ \text{Re} \left[ ir \int_0^{2\pi} d\phi \left( \mathbf{P}_{n,k_z}(\mathbf{r}) \times \nabla \times \mathbf{P}_{n,k_z}^*(\mathbf{r}) \right) \cdot \mathbf{e}_r \right] = 4\delta_{P,P'}. \end{aligned} \quad (\text{A.3})$$

### Appendix B: Scattering of electromagnetic waves from uniaxial cylindrical objects

Consider a wave propagating in an anisotropic medium, with dielectric permittivity tensor (29) and magnetic permeability  $\mu(\omega)$ .

Considering the system's uniaxial symmetry we look for wave-solutions in the form of cylindrical harmonics (A.1),

$$\begin{aligned} \mathbf{RM}_{n,k_z}^{un}(\mathbf{r}) &= \left[ \frac{in}{qMr} J_n(qMr) \mathbf{e}_r - J'_n(qMr) \mathbf{e}_\phi \right] \\ &\quad \times e^{ik_z z + in\phi}, \\ \mathbf{RN}_{n,k_z}^{un}(\mathbf{r}) &= \frac{c}{\omega} \left[ ik_z J'_n(qNr) \mathbf{e}_r - \frac{nk_z}{qNr} J_n(qNr) \mathbf{e}_\phi \right. \\ &\quad \left. + \gamma_N q N J_n(qNr) \mathbf{e}_z \right] e^{ik_z z + in\phi}, \end{aligned} \quad (\text{B.1})$$

where  $\gamma_N$  is some constant which modifies the  $N$ -polarized cylindrical harmonic due to uniaxial anisotropy. Importantly, we do not care about keeping the harmonics (B.1) normalized as that does not influence calculations

of  $\mathbb{T}$  matrix elements in which we are interested. Note that the time dependence  $\exp(-i\omega t)$  is omitted here.

The following Maxwell's equations must be satisfied,

$$\begin{aligned} -\nabla \times \nabla \times \mathbf{RM}_{n,k_z}^{un}(\mathbf{r}) &= \frac{1}{c^2} \left( \hat{\varepsilon} \mu \frac{\partial^2}{\partial t^2} \mathbf{RM}_{n,k_z}^{un}(\mathbf{r}) \right), \\ \nabla \cdot [\hat{\varepsilon} \mathbf{RM}_{n,k_z}^{un}(\mathbf{r})] &= 0, \end{aligned} \quad (\text{B.2})$$

with analogous relations for  $\mathbf{RN}_{n,k_z}^{un}(\mathbf{r})$ .

Substituting expressions (B.1) into equations (B.2), we obtain the following unnormalized wave solutions,

$$\begin{aligned} \mathbf{RM}_{n,k_z}^{un}(\mathbf{r}) &= \left[ \frac{in}{q_M r} J_n(q_M r) \mathbf{e}_r - J'_n(q_M r) \mathbf{e}_\phi \right] e^{ik_z z + in\phi}, \\ \mathbf{RN}_{n,k_z}^{un}(\mathbf{r}) &= \frac{c}{\omega} \left[ ik_z J'_n(q_N r) \mathbf{e}_r - \frac{nk_z}{q_N r} J_n(q_N r) \mathbf{e}_\phi \right. \\ &\quad \left. + \frac{\varepsilon_r}{\varepsilon_z} q_N J_n(q_N r) \mathbf{e}_z \right] e^{ik_z z + in\phi}, \end{aligned} \quad (\text{B.3})$$

where  $q_M$  and  $q_N$  are the wave-vector components perpendicular to the  $z$ -axis for the two solutions respectively,

$$q_M = \sqrt{\varepsilon_r \mu k^2 - k_z^2}, \quad q_N = \sqrt{\varepsilon_z / \varepsilon_r \sqrt{\varepsilon_r \mu k^2 - k_z^2}}. \quad (\text{B.4})$$

One solution is an ordinary wave and is  $M$ -polarized, whereas the other one is called an extraordinary wave and possesses  $N$ -polarization [45].

In order to solve the scattering problem for the cylinder, we expand the electromagnetic field in cylindrical basis (A.1) and (B.3), outside and inside the cylinder respectively. The expansion coefficients for the field inside and outside can be obtained by matching boundary conditions at the cylinder's surface for field components tangential to the surface.

Using the definition of the  $\mathbb{T}$  matrix, we describe the scattering process of a regular magnetic wave by the field outside the cylinder, which is

$$\mathbf{E}_{n,k_z}^{M,out} = \mathbf{RM}_{n,k_z} + T_{n,k_z}^{MM} \mathbf{M}_{n,k_z} + T_{n,k_z}^{NM} \mathbf{N}_{n,k_z} \quad (\text{B.5})$$

and the field inside the cylinder,

$$\mathbf{E}_{n,k_z}^{M,in} = A_{n,k_z}^{MM} \mathbf{RM}_{n,k_z}^{un} + A_{n,k_z}^{NM} \mathbf{RN}_{n,k_z}^{un}. \quad (\text{B.6})$$

Analogously, for an incident electric (TM) multipole field, the field outside the cylinder becomes

$$\mathbf{E}_{n,k_z}^{N,out} = \mathbf{RN}_{n,k_z} + T_{n,k_z}^{MN} \mathbf{M}_{n,k_z} + T_{n,k_z}^{NN} \mathbf{N}_{n,k_z} \quad (\text{B.7})$$

and the field inside the cylinder,

$$\mathbf{E}_{n,k_z}^{N,in} = A_{n,k_z}^{MN} \mathbf{RM}_{n,k_z}^{un} + A_{n,k_z}^{NN} \mathbf{RN}_{n,k_z}^{un}. \quad (\text{B.8})$$

We next derive the specific form of the  $\mathbb{T}$  matrix coefficients by matching the boundary conditions for the medium, i.e. the continuity of  $E_\phi$ ,  $E_z$ ,  $H_\phi$  and  $H_z$  across the cylindrical surface. Plugging the explicit form of cylindrical harmonics (A.1) and (B.3) into these conditions we obtain two sets of four linear equations for the expansion coefficients. Using  $\mathbf{B} = -i(c/\omega)\nabla \times \mathbf{E}$  and  $\mathbf{H} = \mathbf{B}/\mu$  we can write the system of equations for reflection and transmission amplitudes in case of the incident magnetic waves in the form,

$$\mathbb{M}_{n,k_z} \begin{pmatrix} A^{MM} \\ T^{MM} \\ A^{NM} \\ T^{NM} \end{pmatrix}_{n,k_z} = \begin{pmatrix} \frac{c}{\omega} q J_n(qR) \\ J'_n(qR) \\ 0 \\ \frac{nk_z c}{qR\omega} J_n(qR) \end{pmatrix}, \quad (\text{B.9})$$

with the matrix

$$\mathbb{M}_{n,k_z} = \begin{pmatrix} \frac{q_M c}{\mu \omega} J_n(q_M R) & -\frac{q c}{\omega} H_n^{(1)}(qR) & 0 & 0 \\ J'_n(q_M R) & -H_n^{(1)}(qR) & \frac{nk_z c}{q_N R \omega} J_n(q_N R) & -\frac{nk_z c}{q_N R \omega} H_n^{(1)}(qR) \\ 0 & 0 & \frac{\varepsilon_r}{\varepsilon_z} \frac{q_N c}{\omega} J_n(q_N R) & -\frac{q c}{\omega} H_n^{(1)}(qR) \\ -\frac{nk_z c}{\mu q_M R \omega} J_n(q_M R) & -\frac{nk_z c}{q R \omega} H_n^{(1)}(qR) & \varepsilon_r J'_n(q_N R) & -H_n^{(1)}(qR) \end{pmatrix}. \quad (\text{B.10})$$

For the incident electric waves the linear equations are

$$\mathbb{M}_{n,k_z} \begin{pmatrix} A^{MN} \\ T^{MN} \\ A^{NN} \\ T^{NN} \end{pmatrix}_{n,k_z} = \begin{pmatrix} 0 \\ \frac{nk_z c}{q R \omega} J_n(qR) \\ \frac{c}{\omega} q J_n(qR) \\ J'_n(qR) \end{pmatrix} \quad (\text{B.11})$$

The solutions to these sets of equations (B.9) and (B.11) are provided in Eqs. (30)-(37).

### Appendix C: Small $R$ expansion of the $\mathbb{T}$ operator of the cylinder

In order to derive Eqs. (38) and (39), we need the expansion of the  $\mathbb{T}$  operator in terms of  $\omega R/c$ . For a cylinder made of isotropic material with magnetic permeability  $\mu(\omega)$  and dielectric permittivity  $\varepsilon(\omega)$ , we find for the



limit  $R \ll \{\delta, c/\omega\}$ ,

$$T_{0,k_z}^{NN} = -\frac{i\pi}{4}(\varepsilon - 1)(\tilde{k}_z^2 - 1)(\omega R/c)^2, \quad (\text{C.1})$$

$$T_{0,k_z}^{MM} = -\frac{i\pi}{4}(\mu - 1)(\tilde{k}_z^2 - 1)(\omega R/c)^2, \quad (\text{C.2})$$

$$T_{1,k_z}^{NN} = T_{-1,k_z}^{NN} = \frac{i\pi \tilde{k}_z^2 (\mu + 1)(\varepsilon - 1) + (\mu - 1)(\varepsilon + 1)}{4(\varepsilon + 1)(\mu + 1)} \times (\omega R/c)^2, \quad (\text{C.3})$$

$$T_{1,k_z}^{MM} = T_{-1,k_z}^{MM} = \frac{i\pi \tilde{k}_z^2 (\mu - 1)(\varepsilon + 1) + (\mu + 1)(\varepsilon - 1)}{4(\varepsilon + 1)(\mu + 1)} \times (\omega R/c)^2, \quad (\text{C.4})$$

$$T_{1,k_z}^{MN} = T_{1,k_z}^{NM} = -T_{-1,k_z}^{MN} = -T_{-1,k_z}^{NM} = \frac{i\pi}{2} \frac{(\varepsilon\mu - 1)\tilde{k}_z}{(\varepsilon + 1)(\mu + 1)} \times (\omega R/c)^2, \quad (\text{C.5})$$

where  $\tilde{k}_z = k_z/k$ . Substitution of the these forms into Eqs. (22) and (23) yields Eqs. (38) and (39).

#### Appendix D: Leading term of $\mathbb{T}$ operator for $\omega/c \gg R \gg \delta$

For  $\omega/c \gg R \gg \delta$ , the leading term of  $\mathbb{T}$  operator is the  $T_{0,k_z}^{NN}$  element which has then the following form,

$$\lim_{\omega/c \gg R \gg \delta} T_{0,k_z}^{NN} = \frac{-\pi}{\pi + 2i\gamma_E + \frac{2}{(1-\tilde{k}_z^2)(2i+\sqrt{\varepsilon}\omega R/c)} + 2i \log[\sqrt{1-\tilde{k}_z^2}\omega R/2c]}, \quad (\text{D.1})$$

where  $\gamma_E \approx 0.577$  is the Euler-Mascheroni constant. It can be numerically shown that other elements of  $\mathbb{T}$  matrix are negligible.

- 
- [1] M. Planck, Ann. Phys. **4**, 553 (1901).
  - [2] L. Boltzmann, Ann. Phys. **22**, 291 (1884).
  - [3] R. Carminati and J. J. Greffet, Phys. Rev. Lett. **82**, 1660 (1999).
  - [4] Yu. N. Barabanenkov and M. Yu. Barabanenkov, Bulletin of the Russian Academy of Sciences: Physics Volume **72**, Number 1 (2008).
  - [5] M. Laroche, C. Arnold, K. Marquier, R. Carminati and J. J. Greffet, Opt. Lett. **30**, 2623 (2005).
  - [6] N. Dahan, A. Niv, G. Biener, Y. Gorodetski, V. Kleiner, and E. Hasman, Phys. Rev. B **76**, 045427 (2007).
  - [7] M. Laroche, R. Carminati, and J. J. Greffet, J. Appl. Phys. **100**, 063704 (2006).
  - [8] A. Cvitkovic, N. Ocelic, J. Aizpurua, R. Guckenberger, and R. Hillenbrand, Phys. Rev. Lett. **97**, 060801 (2006).
  - [9] D. L. C. Chan, M. Soljacic and J. D. Joannopoulos, Phys. Rev. E **74**, 016609 (2006).
  - [10] G. Biener, N. Dahan, A. Niv, V. Kleiner, and E. Hasman, Appl. Phys. Lett. **92**, 081913 (2008).
  - [11] C. F. Bohren and D.R. Huffman, *Absorption and scattering of light by small particles* (Wiley, Weinheim, 2004).
  - [12] G. W. Kattawar and M. Eisner, Appl. Opt. **9**, 2685–2690 (1970).
  - [13] K. Hansen and E.E.B. Campbell, Phys. Rev. E **58**, 5477 (1998).
  - [14] B. Shapiro, Phys. Rev. B **82**, 075205 (2010)
  - [15] Z. Ruan and S. Fan, Phys. Rev. Lett. **105**, 013901 (2010).
  - [16] Y. Öhman, Nature **192**, 254 (1961).
  - [17] B. Adgur, G. Bling, F. Sellberg and Y. Öhman, Phys. Rev. **130**, 996 (1963).
  - [18] S. Ingvarsson, J. L. Klein, Y. Y. Au, J. A. Lacey, and H. F. Hamann, Opt. Express **15**, 11249 (2007).
  - [19] Y. Y. Au, H. S. Skulason, S. Ingvarsson, L. J. Klein, and H. F. Hamann, Phys. Rev. B **78**, 085402 (2008).
  - [20] O. G. Kollyukh, A. I. Liptuga, V. Morozhenko, V. I. Pipa, and E. F. Venger, Opt. Commun. **276**, 131 (2007).
  - [21] Peng Li, Kaili Jiang, Ming Liu, Qunqing Li, Shoushan Fan, and Jialin Sun, Appl. Phys. Lett. **82**, 1763 (2003).
  - [22] A. E. Aliev and A. A. Kuznetsov, Phys. Lett. A **372**, 4938 (2008).
  - [23] F. Marquier, C. Arnold, M. Laroche, J. J. Greffet, and Y. Chen, Opt. Express **16**, 5305 (2008).
  - [24] G. Bimonte, L. Cappellin, G. Carugno, G. Ruoso, and D. Saadeh, New Journal of Physics **11**, 033014 (2009).
  - [25] Y. Fan, S. B. Singer, R. Bergstrom, and B. C. Regan, Phys. Rev. Lett. **102**, 187402 (2009).
  - [26] S. B. Singer, M. Mecklenburg, E. R. White, and B. C. Regan, Phys. Rev. B **83**, 233404 (2011).
  - [27] S. B. Singer, M. Mecklenburg, E. R. White, and B. C. Regan, arXiv:1107.4061v1.
  - [28] M. Krüger, T. Emig, and M. Kardar, Phys. Rev. Lett. **106**, 210404 (2011).
  - [29] G. Bimonte, Phys. Rev. A **80**, 042102 (2009).
  - [30] R. Messina and M. Antezza, Europhys. Lett. **95**, 61002 (2011); R. Messina and M. Antezza, Phys. Rev. A **84**, 042102 (2011) ;
  - [31] C. Otey and S. Fan, arXiv:1103.2668v1.
  - [32] A. W. Rodriguez, O. Ilic, P. Bermel, I. Celanovic, J. D. Joannopoulos, M. Soljacic, and S. G. Johnson, arXiv:1105.0708v2.
  - [33] M. Krüger, T. Emig, G. Bimonte, and M. Kardar, Europhys. Lett. **95**, 21002 (2011).
  - [34] A. P. McCauley, M. T. H. Reid, M. Krüger, and S. G. Johnson, arXiv:1107.2111v2.

- [35] G. Bimonte, T. Emig, M. Krüger, and M. Kardar, arXiv:1107.1597v1.
- [36] S.M. Rytov, Y.A. Kravtsov and V.I. Tatarskii, *Principles of Statistical Radiophysics 3* (Springer, Berlin, 1978).
- [37] W. Eckhardt, Phys. Rev. A **29**, 1991 (1984).
- [38] S. J. Rahi, T. Emig, N. Graham, R. L. Jaffe, and M. Kardar, Phys. Rev. D **80**, 085021 (2009).
- [39] J. D. Jackson, *Classical Electrodynamics* (Wiley, New York, 1999).
- [40] L. Tsang, J. A. Kong, and K.-H. Ding, *Scattering of Electromagnetic Waves* (Wiley, New York, 2000).
- [41] S.-A. Biehs, F. S.S. Rosa, P. Ben-Abdallah, arXiv:1105.3745v1.
- [42] R. F. Rajter, R. Podgornik, V. A. Parsegian, R. H. French, and W. Y. Ching, Phys. Rev. B. **76**, 045417 (2007).
- [43] J. Lekner, J. Phys.: Condens. Matter **3**, 6121 (1991).
- [44] E. Noruzifar, T. Emig, and R. Zandi, arXiv:1106.4981v1.
- [45] M. Born, E. Wolf, A. B. Bhatia and P. C. Clemmow, *Principles of Optics: Electromagnetic Theory of Propagation, Interference and Diffraction of Light* (Cambridge University Press, 1999).
- [46] W. G. Spitzer, D. Kleinman and D. Walsh, Phys. Rev., **113**, 127 (1959)
- [47] M. A. Ordal, L. L. Long, R. J. Bell, S. E. Bell, R. R. Bell, R. W. Alexander Jr., and C. A. Ward, Appl. Opt. **22**, 1099-1119 (1983).
- [48] S. M. Rytov, *Theory of electric fluctuations and thermal radiation* (Air Force Cambridge Research Center, Bedford, MA, 1959).
- [49] S. Roberts, Phys. Rev. **114**, 104 (1959).
- [50] M. F. Lin, F. L. Shyu, and R. B. Chen, Phys. Rev. B **61**, 14114-14118 (2000).
- [51] A. B. Djuricic, E. H. Li, J. Appl. Phys. **85**, 74047410 (1999).